



Electrophysiological confrontation of Lead-DBS-based electrode localizations in patients with Parkinson's disease undergoing deep brain stimulation

Abdullah Al Awadhi^{a,e}, Rémi Tyrand^{a,e}, Andreas Horn^c, Astrid Kibleur^b, Julia Vincentini^d, André Zacharia^b, Pierre R. Burkhard^{a,b}, Shahan Momjian^{a,e}, Colette Boëx^{a,e,*}

^a Faculty of Medicine, University of Geneva, Geneva, Switzerland

^b Department of Neurology, Geneva University Hospitals, Geneva, Switzerland

^c Movement Disorders and Neuromodulation Section, Department of Neurology, Charité University Medicine, Berlin, Germany

^d École Polytechnique Fédérale de Lausanne (EPFL), Lausanne, Switzerland

^e Department of Neurosurgery, Geneva University Hospitals, Geneva, Switzerland

ARTICLE INFO

Keywords:

Lead-DBS
Microelectrode
Parkinson's disease
Deep brain stimulation

ABSTRACT

Microelectrode recordings (MERs) are often used during deep brain stimulation (DBS) surgeries to confirm the position of electrodes in patients with advanced Parkinson's disease.

The present study focused on 32 patients who had undergone DBS surgery for advanced Parkinson's disease. The first objective was to confront the anatomical locations of intraoperative individual MERs as determined electrophysiologically with those determined postoperatively by image reconstructions. The second aim was to search for differences in cell characteristics among the three subthalamic nucleus (STN) subdivisions and between the STN and other identified subcortical structures.

Using the DISTAL atlas implemented in the Lead-DBS image reconstruction toolbox, each MER location was determined postoperatively and attributed to specific anatomical structures (sensorimotor, associative or limbic STN; substantia nigra [SN], thalamus, nucleus reticularis polaris, zona incerta [ZI]). The STN dorsal borders determined intraoperatively from electrophysiology were then compared with the STN dorsal borders determined by the reconstructed images. Parameters of spike clusters (firing rates, amplitudes – with minimum amplitude of 60 μ V⁻, spike durations, amplitude spectral density of β -oscillations) were compared between structures (ANOVAs on ranks).

Two hundred and thirty one MERs were analyzed (144 in 34 STNs, 7 in 4 thalami, 5 in 4 ZIs, 34 in 10 SNs, 41 others). The average difference in depth of the electrophysiological dorsal STN entry in comparison with the STN entry obtained with Lead-DBS was found to be of 0.1 mm (standard deviation: 0.8 mm). All 12 analyzed MERs recorded above the electrophysiologically-determined STN entry were confirmed to be in the thalamus or zona incerta. All MERs electrophysiologically attributed to the SN were confirmed to belong to this nucleus. However, 6/34 MERs that were electrophysiologically attributed to the ventral STN were postoperatively reattributed to the SN. Furthermore, 44 MERs of 3 trajectories, which were intraoperatively attributed to the STN, were postoperatively reattributed to the pallidum or thalamus.

MER parameters seemed to differ across the STN, with higher spike amplitudes ($H = 10.64$, $p < 0.01$) and less prevalent β -oscillations ($H = 9.81$, $p < 0.01$) in the limbic STN than in the sensorimotor and associative subdivisions. Some cells, especially in the SN, showed longer spikes with lower firing rates, in agreement with described characteristics of dopamine cells. However, these probabilistic electrophysiological signatures might become clinically less relevant with the development of image reconstruction tools, which deserve to be applied intraoperatively.

* Corresponding author at: Department of Neurology, Geneva University Hospitals, Faculty of Medicine, University of Geneva, Rue Gabrielle Perret-Gentil 4 – 1211, Geneva, Switzerland.

E-mail address: Colette.Boex@hcuge.ch (C. Boëx).

<https://doi.org/10.1016/j.nicl.2022.102971>

Received 8 September 2021; Received in revised form 6 January 2022; Accepted 21 February 2022

Available online 25 February 2022

2213-1582/© 2022 Faculty of medicine, University Hospitals of Geneva. Published by Elsevier Inc. This is an open access article under the CC BY-NC-ND license

(<http://creativecommons.org/licenses/by-nc-nd/4.0/>).

1. Introduction

In many centers, electrophysiological mapping using microelectrode recordings is performed during subthalamic nucleus (STN) deep brain stimulation (DBS) surgery in patients with advanced Parkinson's disease (PD) (Gross et al., 2006). This mapping is performed in addition to the main stereotactic targeting using preoperative imaging, to increase the precision of electrode positioning. Three functional subdivisions have been described for the STN (Alexander et al., 1990; Parent and Hazrati, 1995): a dorsolateral part associated with sensorimotor functions; a ventromedial part with associative connectivity; and a medial part with limbic functions. In reality, no clear septa are known to divide the STN and more likely, its divisions are implemented as a gradient. Still, many studies aimed at increasing the accuracy of DBS electrode positioning by searching for electrophysiological signatures of the STN, especially for its sensorimotor subdivision (Gross et al., 2006; Rappel et al., 2020; Seifried et al., 2012).

The electrophysiological pattern of neuronal cells in Parkinson's disease is usually described as bursty, irregular, tonic or oscillatory (Benazzouz et al., 2002; Rodriguez-Oroz et al., 2001). Their frequency, shape and duration, including their positive and negative phases, were also analyzed with the objective of identifying the nature of cells, e.g. dopaminergic or GABAergic (Matsumoto and Hikosaka, 2009a). The dorsolateral STN was first identified from microelectrode recordings (MERs) in response to movements (Abosch et al., 2002; Theodosopoulos et al., 2003). It was shown to present the highest proportion of bursty and oscillatory cells within the STN (Seifried et al., 2012). Also, β -oscillations measured either from MERs (Levy et al., 2002; Steigerwald et al., 2008) or from local field potentials (Brown et al., 2001; Levy et al., 2002) were shown to be mainly located in the dorsolateral STN (Alavi et al., 2013; Zaidel et al., 2010). Similar MER frequency analyses were performed in an attempt to bring out the differences between the ventral and dorsal subdivisions (Deffains et al., 2014; Pozzi et al., 2016). Finally, spatial differences were more clearly found with local field potentials which also revealed an important theta-alpha [7–10 Hz] region in the ventral STN, corresponding to the limbic subdivision (Rappel et al., 2020).

Recently, methods for accurate electrode localizations based on pre- and postoperative imaging were introduced. For instance, in the last few years, the Lead-DBS image reconstruction toolbox (Horn and Kuhn, 2015a; Horn et al., 2019) has been made available as an open-source software (<https://www.lead-dbs.org>). This tool allows, in particular, the fusion of magnetic resonance images (MRIs) with computed tomography (CT) scans and the display of DBS electrodes along the surgical trajectory in patients with PD. In addition, this tool allows the superposition of different anatomical atlases. This helps to highlight the electrodes' relationship with different neuroanatomical substrates, such as the subthalamic nucleus (STN). In particular, the DISTAL atlas displays the STN and its subdivisions; the substantia nigra (SN), located ventrally to the STN; the thalamus and its subdivisions, as well as the zona incerta (ZI), both located dorsally to the STN (Ewert et al., 2018). This subcortical atlas was based on manual segmentations of high resolution brain template series, the Montreal Neurological Institute (MNI) 152 template series, to which a histological atlas and an atlas of structural connectivity were co-registered (Ewert et al., 2018).

The present retrospective study focused on the intraoperative MERs of a group of 32 patients with PD who have undergone STN-DBS surgery, which were postoperatively assigned to a neuroanatomical structure using Lead-DBS. The first aim was to evaluate the accuracy of the DISTAL atlas implemented in Lead-DBS by analyzing the concordance of each MER's anatomical localization as determined by their electrophysiological signature with that determined by Lead-DBS. Secondly, the observation of occasional cells with high spike amplitudes upon reaching the STN motivated us to search for differences in MER parameters first between the STN's subdivisions, and then between the STN and the surrounding structures.

2. Materials & methods

2.1. Patients

The study was authorized by the local Ethics Committee (CE N°2018-02100). All participants signed a consent form to be included. It was conducted following the recommended ethical guidelines of the Declaration of Helsinki.

Thirty-two patients with PD who consecutively underwent STN-DBS, for whom imaging and microelectrode recordings were available, were included retrospectively (13 females, 19 males). The median age was 62 years (interquartile range: 56.7–67.0 years), the youngest subject being 45 years old and the oldest 74 years old at the time of surgery. The median age at illness onset was 52.0 years (interquartile range: 46.5–55.7 years).

The motor outcomes, evaluated pre-operatively and one year post-surgery using the Movement Disorders Society-Unified Parkinson's Disease Rating Scale (MDS-UPDRS) part III (OFF-drug condition pre-surgery; OFF-drug/ON-stimulation condition post-surgery), are listed in [Inline Supplementary Table 1](#); preoperative: mean 38.7, standard deviation 13.5; postoperative: mean 17.5, standard deviation 9.1).

2.2. Targeting and surgical procedure

Stereotactic targeting was performed by neurosurgeons with preoperative 3 Tesla T2 and gadolinium-enhanced T1 MRIs merged with a CT scan (Leksell® Coordinate Frame G Kit [Elekta, Stockholm, Sweden]). Trajectory determination was made using Brainlab iPlan Stereotaxy.

A description of the surgical intervention can be found in a previous study (Boëx et al., 2018). The Neurostar DBS-Guide system was used (Neurostar, Tübingen, Germany). The microelectrodes were positioned using a Ben-Gun five-microelectrode holder, offering posterolateral or anterolateral and posteromedial or anteromedial trajectories, in addition to the central trajectory. During the procedure, patients were awake as the electrodes were implanted and as neurologists clinically assessed the effects of intraoperative macrostimulation on rigidity and muscle group contractions.

The trajectory chosen for placing the definitive electrode was selected mainly based on the efficacy of macrostimulation on rigidity (Boëx et al., 2018). The electrode was generally positioned centering its contacts 1.5 mm below the STN entry, intraoperatively determined from MERs as described further below. This depth was also the stimulation site for the assessment of rigidity changes. Thus, for instance, in the case of a Lead 3389 electrode (Medtronic Inc, Minneapolis, MN, USA), 2 contacts were located just above stimulation site, with the upper limit of contact number 2 located at the dorsal STN entry point, and 2 contacts below the stimulation site. In addition, the positioning of the definitive electrode was made under fluoroscopy with a stored reference of the stimulation site position. Hence, the location of the definitive electrode was carefully monitored intraoperatively in relation with the depths of each MER (mm) with the known depth of stimulation, i.e. center of the definitive electrode, verified again with fluoroscopy. Twenty-seven patients received the Lead 3389 electrode (Medtronic Inc, Minneapolis, MN, USA), and five the non-directional Vercise electrode (Boston Scientific, Marlborough, MA, USA).

2.3. Microelectrode recordings (MERs)

For each patient, the number of microelectrodes (microTargeting electrode, Pt/Ir [FHC, Bowdoin, Maine, USA]) to be used was chosen depending on the anatomy seen on preoperative imaging. For most STNs, 2 microelectrodes were introduced simultaneously (usually one with a central trajectory, one with a posterolateral trajectory, and sometimes a third track was added, most frequently with a posteromedial trajectory). During the descent, spikes were recorded at every level, millimeter per millimeter down to 2 mm before the estimated STN

entrance. From there, spikes were recorded within 0.3 mm steps. The patients were kept fully awake and could talk from time to time to the clinicians. It was not recorded however if, for instance, the patients were eyes closed or not at the time of recordings.

The MERs were performed using the Neurostar DBS-Guide and NeuroBook systems (Neurostar, Tübingen, Germany). They were interpreted after amplification ($\times 10,000$; band-pass filter: 4th order Butterworth filter, 300–5,000 Hz) and digitization (12 bits; 20,000 Hz). Every MER's depth (in millimeters) was carefully marked down at the time of exploration. With the Neurostar Microdrive DBS-Guide, depths are negative above target (0 mm) and positive beyond.

Intraoperative STN mapping was determined by an electrophysiologist (C.B.) based on the MERs, applying the original description by Rodriguez-Oroz et al., (Rodriguez-Oroz et al., 2001), and by Benazzouz et al. (Benazzouz et al., 2002). Entrance into the STN was characterized by the first bursting or random firing neurons, and exit from the STN was determined by the disappearance of neuronal signals or by the recognition of SN cells (more regular, with higher firing rates).

2.4. Pre-processing and electrophysiological parameters

Spike detection, sorting, and clustering were carried out by applying the method developed by Quiroga et al. (Quiroga et al., 2004). After visual verification of the spike clusters, some were re-clustered, as appropriate, especially when this verification step brought out multi-unit recordings. Only the MERs that lasted at least 45 sec, necessary for reliable planned pattern analyses (Sharott et al., 2014), and that showed spike clusters with a minimum peak-to-peak amplitude of 60 μV , to avoid the confusion of cells with electrical noise, were included. The considered electrophysiological parameters of each cell were the

following: the global firing rate of spike clusters, expressed as the number of spikes per second computed over the whole recording duration; the mean amplitude of spikes, measured as the mean of the peak-to-peak amplitudes of a cluster's spikes; the duration of the negative and positive phases of a cluster's spikes, measured as the durations between consecutive crossing zero amplitudes of spikes; and the amplitude spectral density of β -oscillations. An example of a spike cluster is given in Fig. 1.

The spectral power of β -oscillations was computed from the MERs, as first described by Zaidel et al. (Zaidel et al., 2009). First, the longest stable period of each recording was determined by computing the root mean square on moving time windows of 50 ms duration. Only the longest consecutive time series lying between the median root mean square value and 2 standard deviations was used for the next steps of analyses. Welch power spectral density was then estimated on the absolute value of the demeaned time series. The spectral estimate was normalized at each frequency by the total power in the 2–200 Hz range, and finally the amplitude of the spectral power of β -oscillations (13–31 Hz) was extracted.

2.5. Postoperative image reconstruction

The default pipeline (Horn et al., 2019) using the Lead-DBS Matlab toolbox (<https://www.lead-dbs.org/>) (Horn and Kühn, 2015b) v2.1.7 was applied. Advanced normalization tools (ANTs; <https://stnava.github.io/ANTs/>) (Avants et al., 2011) allowed to co-register the brain images, combining the preoperative 3D T1-weighted (TR = 1930 ms, TE = 2.36 ms, slice thickness: 1 mm), T2-weighted (TR = 2400 ms, TE = 225 ms, slice thickness: 1 mm), and FLAIR (TR = 5000 ms, TE = 386 ms, slice thickness: 1 mm) MRIs (Skyra 3.0T scanner, Siemens Medical

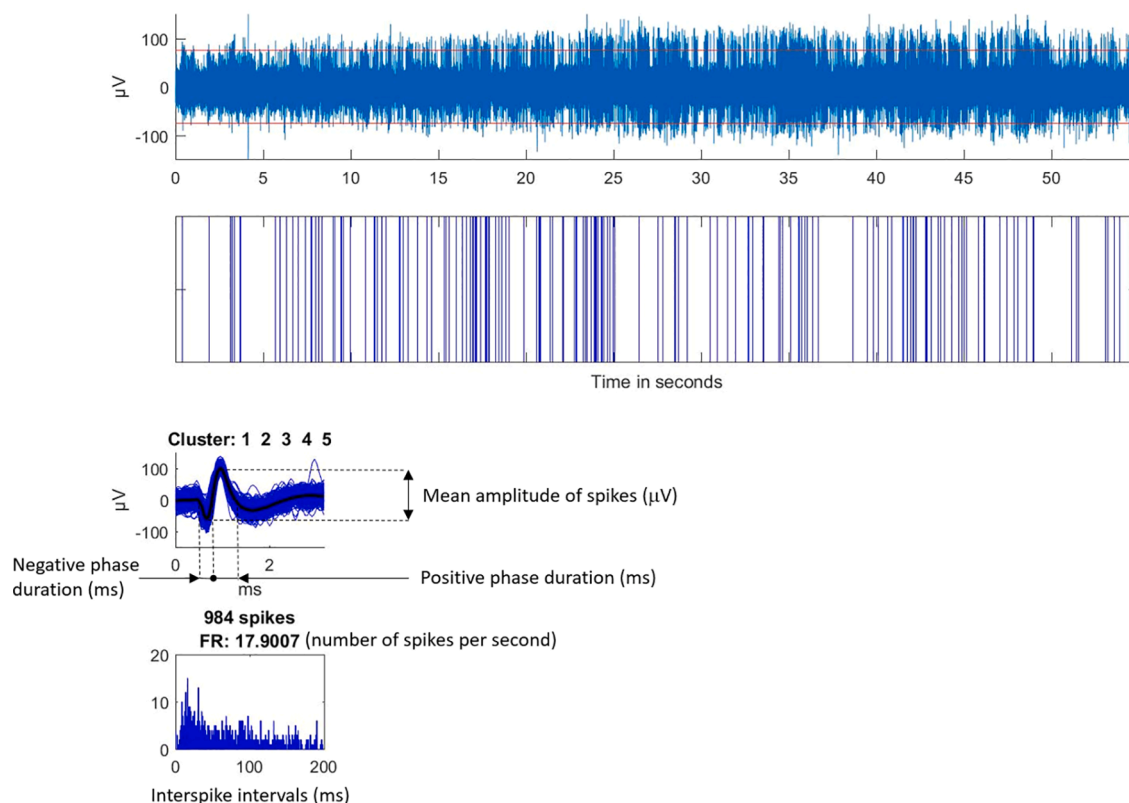


Fig. 1. Illustration of a microelectrode recording analysis with an example of cell recording located in the sensorimotor subdivision of the subthalamic nucleus, where the firing rate is equal to 17.9 spikes per second, the mean amplitude of spikes to 174 μV , and the negative and positive phases of spikes last 0.3 ms and 0.5 ms, respectively. Top graph: raw microelectrode recording. Middle graph: spike waveforms obtained with the clustering of the microelectrode recording (the number of spikes and the firing rate [FR] are also indicated). Bottom graph: interspike interval histograms (ordinate number of times that the delay between two consecutive spikes is within the time category given on the x-axis, with categories of 1 ms).

Systems, Erlangen, Germany) with the postoperative CT scan performed the day after surgery (no other CT scan was performed later; slice thickness between 0.6 and 1.25 mm; pixel spacing: 0.453/0.453; Somatom Definition Flash, Siemens Medical). After co-registration, Lead-DBS performed an automatic correction for brain shifts (Schönecker et al., 2009). Then, based on the preoperative volumes, the symmetric image normalization Diffeomorphic Mapping method (Avants et al., 2008) was used to compute a multispectral normalization to the ICBM 2009b Nonlinear Asymmetric space (Montreal Neurological Institute, MNI) (Fonov et al., 2011). The Unified Segmentation method (Ashburner and Friston, 2005) of the Statistical Parametric Mapping software (SPM12; <https://fil.ion.ucl.ac.uk/spm/>) (Friston et al., 1994) was adopted when the previous approach was unsuccessful. Finally, the PaCER method was applied to automatically pre-construct the DBS electrodes and their contacts (Husch et al., 2018).

To determine the location of each MER relative to the anatomical substrates, the reconstructed images were segmented using the DISTAL atlas (Ewert et al., 2018), bringing out all the relevant subcortical structures, including the STN subdivisions. This subcortical atlas was based on manual segmentations of multimodal (T1, T2, proton density, T2 relaxometry) high resolution brain template series, the Montreal Neurological Institute (MNI) 152 template series (<http://www.bic.mcgill.ca/ServicesAtlases/ICBM152Nlin2009>), to which a histological atlas and an atlas of structural connectivity were co-registered (Ewert et al., 2018). The STN subdivisions using the DISTAL atlas can be brought out using three different representations: either “minimal”, “medium” or “complete”. The “medium” representation of the STN according to the DISTAL atlas was used. Knowing the MERs’ depths (mm) in reference to the carefully marked depths on the definitive electrode (see § 2.2.), each MER could then be localized and attributed to one of the subdivisions of the STN or to one of the other subcortical structures (Fig. 2), that is: the SN (ventral to the STN), the thalamus (dorsal to the STN), the nucleus reticularis polaris (surrounding and enfolding the thalamus), and the ZI (dorsal to the STN).

2.6. Statistical analyses

The entry into the STN was determined intraoperatively from MERs

as the depth at which the first spikes with an amplitude $> 60 \mu\text{V}$ were detected. This electrophysiological landmark was considered as the ground truth, a reference to compare to the STN entry depth determined with the DISTAL atlas (Ewert et al., 2018) for the same trajectory.

Pearson correlations were computed to determine whether the electrophysiological parameters were independent, and each variable was tested for normality (SigmaPlot, Systat Software, Inc., San Jose, California, USA).

ANOVAs on ranks (Kruskal-Wallis One Way Analysis of Variance on ranks) were performed to analyze for possible electrophysiological differences within the STN between its 3 subdivisions, and to compare the whole STN and the surrounding deep nuclei. If a statistically significant difference was found between the subdivisions of the STN, post hoc pairwise multiple comparisons using Dunn’s Method were carried out. If a statistically significant difference was found among the deep brain nuclei, post hoc multiple comparisons were carried out using Dunn’s Method, but this time confronting the whole STN to the surrounding nuclei.

2.7. Data and code availability

The Matlab code, other than the Lead-DBS imaging-reconstruction toolbox (www.lead-dbs.org) used for data analyses and the raw data (electrophysiological and imaging) will be shared by request to C.B., respecting the limitations of the University Hospitals of Geneva through the University of Geneva (<http://www.kheops.ch/>).

3. Results

3.1. Concordance between MER locations, determined by electrophysiology and by imaging-based reconstructions

The distribution of all 231 MERs according to the structures where they were found is given in Table 1. The localization of every MER, reconstructed with Lead-DBS using the DISTAL atlas (Ewert et al., 2018), revealed 144 MERs in the STN (62.3 % of all MERs, 34 STNs, 24 patients), distributed among the sensorimotor (117 MERs, 81.2 % of STN MERs, 26 STNs, 20 patients), the associative (22 MERs, 15.3 % of STN

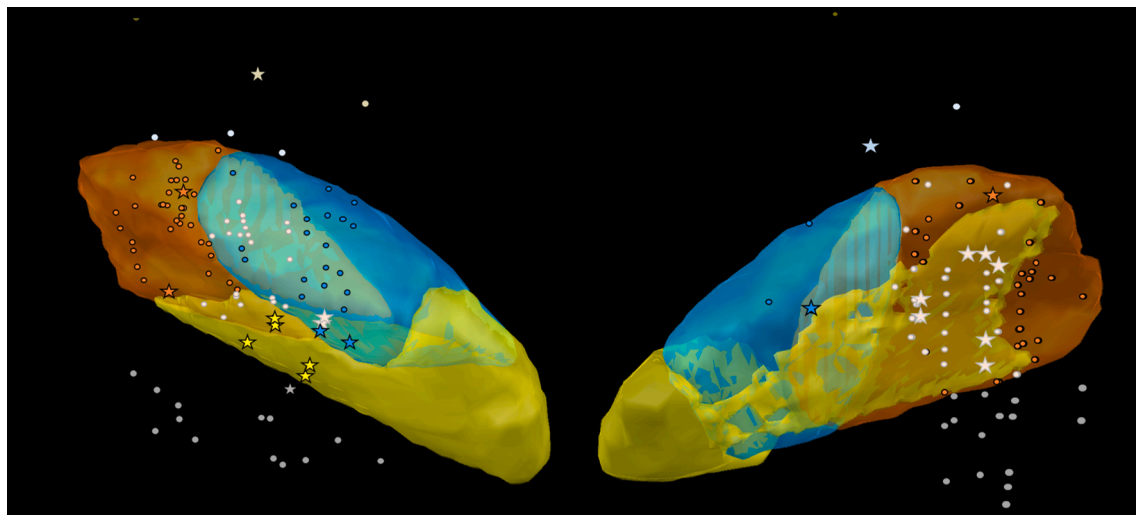


Fig. 2. Image reconstruction of the location of every microelectrode recording (MER) relative to the subthalamic nucleus (STN). The reconstruction was performed with Lead-DBS, using the medium DISTAL atlas (Ewert et al., 2018), and represents both STNs from an anterior view (Orange: sensorimotor STN; Blue: associative STN; Yellow: limbic STN). The location of all MERs are indicated with colored dots (Orange: sensorimotor STN; Pink: sensorimotor behind the limbic or associative subdivisions; Blue: associative STN; Yellow: limbic STN; Grey: substantia nigra, SN; Light blue: zona incerta; Light khaki: thalamic ventro-oralis anterior nucleus, Voa; Khaki: thalamic ventro-oralis posterior nucleus, VLa). Star symbols indicate the location of MERs for which the measured mean amplitude of spikes was above one standard deviation of the mean amplitude of all spikes. Note that not all MERs of the Voa, VLa and SN are represented to limit the extension of the figure. Also, more than one STN MERs can be superimposed on the same position). (For interpretation of the references to colour in this figure legend, the reader is referred to the web version of this article.)

Table 1

Distribution of all 231 MERs relatively to the structure where they were found using the DISTAL atlas.

| Location and global number of MERs | | Number of MERs 231 | Number of structures where the MERs were recorded, with their side (L/R) | Number of patients in whom were recorded these MERs |
|------------------------------------|--|--------------------|--|---|
| STN | Sensorimotor | 117 | 26 | 20 |
| | 144 MERs (62.3%) | (81.2%) | 12 L/14 R | |
| | Associative | 22 | 9 | 8 |
| | 34 STNs (15.3%) | (15.3%) | 3 L/6 R | |
| 24 patients | Limbic | 5 | 2 | 2 |
| | | (3.5%) | 0 L/2 R | |
| Thalamic | Ventro-oralis posterior nucleus (VL _a) | 4 | 3 | 3 |
| | 7 MERs (3.0%) | | 2 L/2 R | |
| | Ventro-oralis anterior nucleus (Voa) | 3 | 3 | 3 |
| 4 thalami patients | | | 1 L/3 R | |
| Zona incerta | | 5 | 4 | 4 |
| | (2.2%) | | 1 L/3 R | |
| Substantia nigra | | 34 | 10 | 7 |
| | (14.7%) | | 4 L/6 R | |
| GPe | | 14 | 1 L | 1 |
| GPi | | 13 | 1 L | 1 |
| Nucleus reticularis polaris | | 12 | 1 R | 1 |
| Internal capsule | | 2 | 1 R | 1 |

For each different structure, the number of MERs are indicated with the number of left (L) or right (R) structures, and the number of patients.

MERs, 9 STNs, 8 patients) and the limbic (5 MERs, 3.5 % of STN MERs, 2 STNs, 2 patients) subdivisions (Fig. 2, N.B. a few STN MERs in different patients were found at the same location). Forty-six MERs were localized in 4 other adjacent structures. Seven MERs were localized in the thalamus (3.0 % of all MERs, 4 thalami, 3 patients: 4 MERs in the ventro-oralis posterior nucleus, VL_a; 3 MERs in the ventralis oralis anterior

nucleus, Voa). Among these 7 MERs, 3 belonged to a patient for whom both trajectories of one side did not pass through the STN at all (not shown in Fig. 2). In that patient, MERs were intraoperatively assigned to the STN, but were re-assigned to the VL_a and the Voa by the postoperative image reconstruction. Then, still above the STN entry, 5 MERs were localized in the ZI (2.2 % of all MERs, 4 ZIs, 4 patients; Fig. 2). Finally, after exiting the STN, ventrally, 34 MERs were localized in the SN (14.7 % of all MERs, 10 SNs, 7 patients; Fig. 2, N.B. some SN MERs were found at the same location for different patients). Intraoperatively, 6/34 MERs of the SN had been attributed to the STN.

Figure 3 illustrates the location of all the definitive DBS electrodes for which MERs were localized in the STN (34 trajectories in 23 patients; 21 right, and 13 left trajectories; corresponding to 19 trajectories in 14 patients first implanted in the right STN, and 15 trajectories in 9 patients first implanted in the left STN). The difference between the depth of the STN entry determined intraoperatively from MERs and the depth of the STN entry determined postoperatively from the reconstructed position of the definitive implanted DBS electrode using the DISTAL atlas (Ewert et al., 2018) was computed for every couple “definitive electrode – implanted MER trajectory”. The average difference in the STN entry depth was found to be of 0.11 mm (standard deviation: 0.8 mm), meaning that the average STN entrance found with the atlas was slightly above the one found with MERs (Inline Supplementary Figure 1). In addition, image reconstructions being performed with the postoperative CTs made usually on the first postoperative day, additional post hoc analyzes were performed to test whether a possible pneumocephalus did affect the differences of STN entry depth found between both methods. After these post hoc analyses, there was no significant difference ($p > 0.1$).

All MERs located above the electrophysiologically-determined STN entry were indeed found to be located in the thalamus or the ZI with the DISTAL atlas.

In Fig. 4, the firing rate, the amplitude and negative phase duration of STN spikes, as well as the β -oscillations are plotted according to their anatomical site of recording, determined using the DISTAL medium atlas (Ewert et al., 2018). The x-axis indicates the MER depths along the

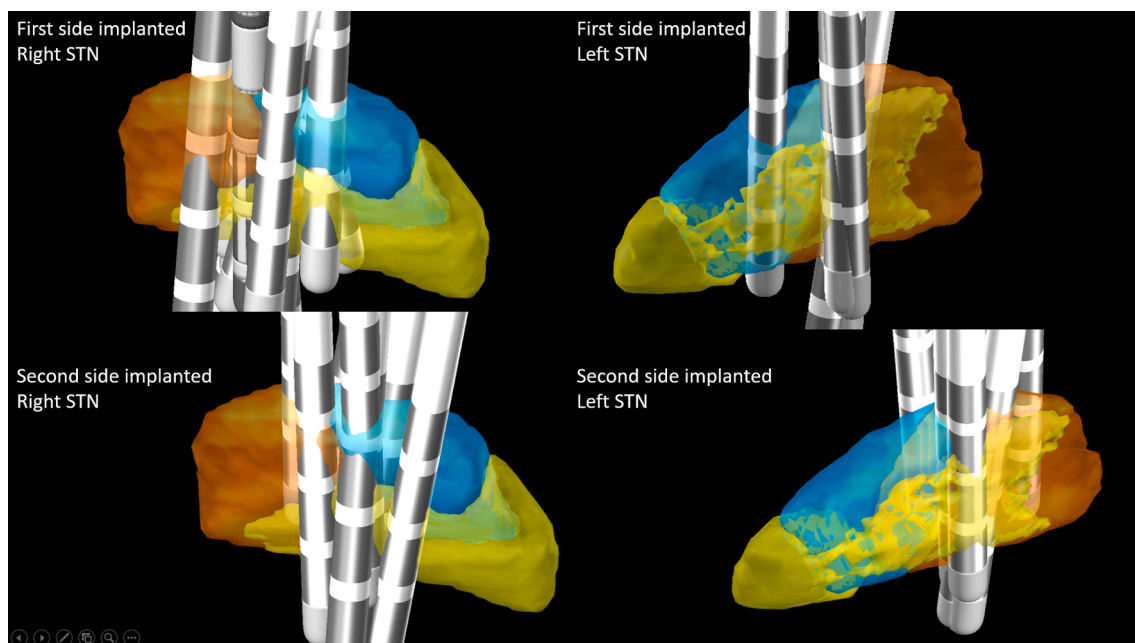


Fig. 3. Image reconstruction of the deep brain stimulation (DBS) electrodes that went through the subthalamic nucleus (STN) and that were located on the microelectrode explorative trajectories selected for the definitive DBS electrode implantation. The reconstruction was performed with Lead-DBS, using the DISTAL atlas (Ewert et al., 2018). From upper left to lower right: the right STN when it was the first side to be implanted; the left STN when it was the first side to be implanted; the right STN when it was implanted after the left STN; the left STN when it was implanted after the right STN. Blue: associative STN; Yellow: limbic STN; Orange: sensorimotor STN. (For interpretation of the references to colour in this figure legend, the reader is referred to the web version of this article.)

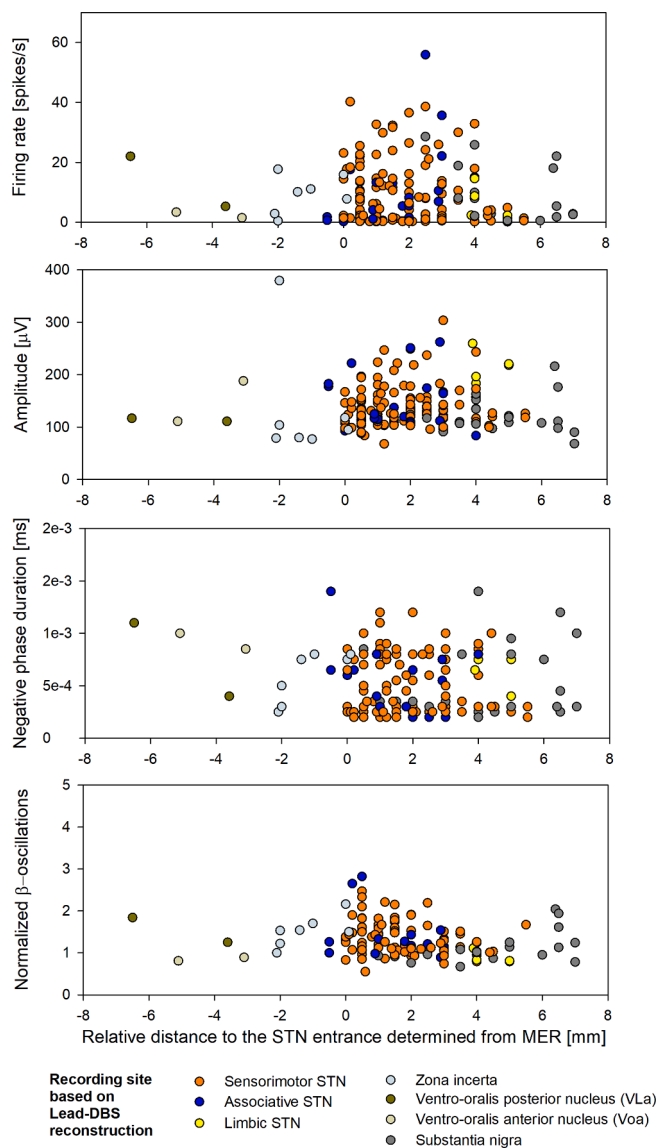


Fig. 4. Distribution of firing rate (first plot), amplitude (second plot), negative phase duration (third plot), and β -oscillations (bottom plot) in relation to the recording depth, for each MER coming from trajectories that passed through the STN. In each plot, the data of the whole group of patients is shown, and each symbol represents a single recording in one patient. On the x-axis, the MER depths are given with the STN entry as the reference depth (0 mm), as determined intraoperatively by electrophysiology. Depths < 0 mm are located above the STN entry point along the explorative trajectory, and depths > 0 mm are located below the STN entry point along the explorative trajectory (with the Neurostar Microdrive DBS-Guide, depths are negative above target (0 mm), and positive beyond target).

explorative trajectories, with the STN entry as the reference depth (0 mm), as determined intraoperatively by an electrophysiologist (C.B.): depths at < 0 mm are located above the STN entry point, whereas depths at > 0 mm are located below the STN entry point along the explorative trajectory (as fixed with the used Microdrive).

Forty-one MERs (17.8 % of MERs) from both trajectories of both sides in one patient were all located outside of the STN (14 in 1 external globus pallidus, GPe; 13 in 1 internal globus pallidus, GPi; 12 in 1 nucleus reticularis polaris; 2 in 1 internal capsule; [Inline Supplementary Figure 2](#)). For this patient, MERs that were intraoperatively attributed to the STN were located in the GPe and the GPi by the postoperative image reconstruction. In addition to Lead-DBS, this unexpected result was also verified using the Brainlab iPlan Stereotaxy tool. This patient was the

only one with recordings of the GPe, the GPi, the nucleus reticularis polaris as well as the internal capsule, and was thus excluded from further statistical analyses.

3.2. Differences across the STN and between the STN and other subcortical regions

The duration of the positive phase of spikes was found to be correlated with the firing rate ($R^2 = -0.3$, $p < 0.001$; [Inline Supplementary Figure 4](#)). This link was due to some cells, of the SN in particular, that showed long positive phase durations of spikes and low firing rates. Because of this link, the positive phase duration was knowingly not included in further analyses.

Only the spike amplitudes and β -oscillations were found to be different across the STN (amplitudes: $H = 10.64$, $p < 0.01$; β -oscillations: $H = 9.81$, $p < 0.01$). The amplitude was found to be higher in the limbic subpart (median = 217.8 μV ; interquartile range (IR): [190.7–243.3 μV]) than in the sensorimotor (median = 132.7 μV ; IR: [116.1–154.8 μV]) and the associative subdivisions (median = 130.3 μV ; IR: [114.1–180.4 μV]), with differences of ranks of 61.53 and 56.49, respectively ($p < 0.05$). Ad hoc analyses of the location of the highest amplitudes of spike (i.e. amplitudes higher than the mean plus one standard deviation of spikes in [Fig. 2](#); higher than 185 μV : 141.2 $\mu\text{V} + 43.8 \mu\text{V}$), are marked by star symbols instead of circles in [Fig. 2](#). These high amplitudes were found in 15 cases, either in the limbic subregion or directly adjacent to the limbic subregion, as provided using the medium DISTAL atlas (one single case in the Voa; one single case in the ZI). The β -oscillations were found to be significantly less prevalent in the limbic subdivision (median amplitude spectral density = 0.83, IR: [0.81–0.97]) than in the sensorimotor (median = 1.24, IR: [1.05–1.53]) and the associative subdivisions (median = 1.26, IR: [1.10–1.51]), with differences of ranks of 58.16 and 62.48, respectively ($p < 0.05$). On the other hand, the firing rate as well as the negative phase duration were not found to differ.

Comparing the electrophysiological parameters among the deep brain nuclei, a significant difference was found only for the β -oscillations ($H = 15.40$, $p < 0.005$). However, the post hoc multiple comparisons confronting the STN to other surrounding nuclei did not bring out any significant difference in β -oscillations. The firing rate, the mean amplitude of spikes, as well as the negative phase duration of spikes did not differ between the analyzed nuclei, including the STN.

4. Discussion

4.1. Electrode localizations

The localization of MERs based on imaging was consistent with intraoperative electrophysiological mapping for determining the dorsal border of the STN, based on MER firing patterns, thus cross-validating the reliability of both methods for this purpose. The first MERs that were postoperatively located in the STN were recorded at the electrophysiological STN entry zone, as indicated by the small average difference found between the depth of the STN entry determined intraoperatively from MERs and the depth of the STN entry determined postoperatively from the reconstructed position of the implanted DBS electrode using the DISTAL atlas. Such high agreement has recently been described by others, as well ([Rappel et al., 2020](#)).

Recently, [Nowacki et al. \(Nowacki et al., 2018\)](#) analyzed the accuracy of DBS electrode locations using atlases provided within the Lead-DBS package: in all regards, the DISTAL atlas ([Ewert et al., 2018](#)), which was used here, was the most accurate atlas. However, this group showed that, although very close, the STN length was significantly different when comparing the measurement performed using the DISTAL atlas and the one obtained from MERs. In particular, the reconstructed DBS electrodes were found too laterally after normalization to the MNI space and atlas application as compared to the native space and the MERs. In

the present study, the MERs could not be used to validate the STN length found with the Lead-DBS reconstruction, as the distinction between ventral STN MERs and SN MERs was not so clear based on electrophysiology. However, our study showed that MERs and Lead-DBS were consistent in determining the STN entry.

Also, Kim et al. (Kim et al., 2019) analyzed the distances of active contacts to the STN's center of mass using reconstructions made with the DISTAL atlas and 7 Tesla MRIs. They found a larger average distance difference when computed with the DISTAL atlas than when using 7 Tesla imaging. The difference was of 3.5 mm, well above the maximum difference found in our series for the STN entry (average 0.11 mm, max 1.5 mm). A difference of 3.5 mm, i.e., three times the diameter of the DBS electrode, is not supported by our results, as illustrated by Fig. 3. The use of 7 Tesla imaging also recently showed that this new field led to determining the localization of the STN's entry more dorsally than determined from MERs (Bot et al., 2019), or to identifying the standard target as more ventral than expected with 3 Tesla imaging (Isaacs et al., 2021). This could reflect a low density of cells at the STN's border that can correspond to the usual increases in background "noise" activity in the MERs observed on the borders of the STN.

It should be recalled that the reconstructed position of the DBS electrode was performed with the postoperative CTs made usually on the first postoperative day. Post hoc analyzes showed that the occurrence of pneumocephalus did not affect the differences found between the depth of the STN entry determined intraoperatively from MERs and that determined postoperatively from the reconstructed images.

All other MER locations determined by Lead-DBS were found to match electrophysiology, except in two patients for whom doubts about the MER locations had already been raised intraoperatively. For these two patients, neither the MERs nor the macrostimulation allowed to identify the location of 3 electrodes, and the image reconstruction using Lead-DBS confirmed that the DBS leads were misplaced. In one of these two patients, MERs were eventually found to belong either to the GPe or to the GPI. This lateral shift could be explained by coordinate errors during the setup of the stereotactic frame. However, this patient still benefited from the procedure, with a GPe-DBS leading to an excellent 80 % motor improvement (considering the motor subscores of the Movement Disorders Society-Unified Parkinson's Disease Rating Scale part III, OFF-drug/ON-stimulation one-year post-surgery of 4.5, versus OFF-drug pre-surgery of 38). The efficacy of this GPe-DBS was in agreement with previous animal models (Vitek et al., 2012). In the second patient, the DBS electrode passed through the VL_a and Vo_a subdivisions of the thalamus, and the stimulated contacts have eventually been located in the VL_a by the Lead-DBS reconstruction, with no long-term benefit. Again in this case, the misplacement may have been due to stereotactic frame coordinate errors.

4.2. Electrophysiological parameters

By comparing the electrophysiological parameters among the STN subdivisions, the amplitude of spikes was found to be higher in the limbic than in the sensorimotor and associative subdivisions. This result, although found with a low number of MERs from the limbic STN (the limbic MERs represented only 3.5 % of the total number of STN recordings), was reinforced by the observation that the highest amplitudes of spikes were found in the limbic subregion or directly adjacent to it. The spatial location of these spikes with high amplitudes suggests that these high amplitudes, i.e. amplitudes of extracellularly recorded action potentials, related to the strength of the field generated by the recorded neuron, were not solely dependent on the distance of the electrode from the cell body. These high amplitude spikes could also be due to an important neuronal excitation of the limbic pathway, in the particularly stressful situation of awake cranial surgeries. They could also be due to the excitation of a particular population of STN neurons in this region. Hence, the reported relationship between the amplitude of spikes and the STN subdivisions could also be secondary to one of these factors.

β -oscillations were less present in the limbic STN, in agreement with previous studies showing a topographical attenuation of β -oscillations following a dorsoventral gradient within the STN (Alavi et al., 2013). Again, this could be related to the reduced impact of PD pathophysiology on the limbic basal ganglia-cortical loop and limbic STN (Irmén et al., 2019; Redgrave et al., 2010; Richardson, 2019). Notably, in addition to spike amplitudes, β -oscillations could be of importance not only in DBS for PD, wherein the limbic STN should be avoided to prevent psychiatric side effects, but also in DBS for other disorders such as obsessive-compulsive disorder, wherein the limbic STN is a target of choice (Mallet et al., 2008; Rappel et al., 2020).

When comparing different deep brain nuclei encountered during DBS surgeries (i.e. Vo_a, VL_a, ZI, and SN) with the STN, no difference in β -oscillations was detected. Indeed, β -oscillations are not specific to the STN, rather, they are highly present throughout the basal ganglia and the cortex of PD patients (Brown et al., 2001; Levy et al., 2002). β -oscillations should thus be considered as a trajectory marker rather than a specific STN marker. Similarly, none of the other parameters differed among the subcortical structures.

Focusing on the firing rate, no difference was found between the STN subdivisions. If a difference in the firing rates across subdivisions of the STN does exist, it is still unclear and controversial (Deffains et al., 2014; Pozzi et al., 2016). The present work, done with a careful attribution of each MER to one of the STN subdivisions, adds doubt about the existence of a firing rate difference among the STN's subparts in patients with PD.

Nevertheless, a strong link was found between the positive phase duration of spikes and the firing rate, especially in the SN where some cells showed particularly long phase durations of spikes and low firing rates. This could suggest a characteristic of dopamine cells, which would be expected in the SN, as was earlier described by Matsumoto and Hikosaka in animal models (Matsumoto and Hikosaka, 2009b). In human patients, the intraoperative firing rate in combination with the waveform duration was suggested as being a potential parameter for distinguishing dopaminergic neurons of the pars compacta subregion from GABAergic neurons of the pars reticulata subregion (Ramayya et al., 2014). Further studies focusing on this aspect are needed and could help identify dopamine neurons in humans based on this characteristic.

5. Conclusions

Imaging-based reconstruction was in agreement with the electrophysiological mapping in determining the dorsal STN entry with an infra-millimetric precision. The Lead-DBS toolbox also allowed us to identify misplaced electrodes, notably revealing a particular case with a clinically successful GPe-DBS. The present study supports that Lead-DBS is reliable in precisely determining the position of DBS electrodes.

Furthermore, some simple electrophysiological parameters differed among functional subregions of the STN. Spike amplitudes were higher in the limbic area of the STN. The study further confirms that the functional subdivisions of the STN differ in terms of β -oscillations, which are slightly more present in the sensorimotor and associative subparts than in the limbic subdivision. Thus, both spike amplitudes and β -oscillations may help to electrophysiologically distinguish STN subdivisions and therefore improve intraoperative targeting and DBS lead positioning. However, these probabilistic electrophysiological signatures are becoming clinically less relevant with the development of new image reconstruction tools, which now deserve to be applied intraoperatively.

Funding

This work was partly supported by the Swiss National Science Foundation [SNF grant no. 320030-149804].

A.H. received funding from the Deutsche Forschungsgesellschaft (Grant no. 410169619). The other authors declare no competing

interests.

CRedit authorship contribution statement

Abdullah Al Awadhi: Conceptualization, Formal analysis, Investigation, Methodology, Project administration, Software, Validation, Visualization, Writing – original draft, Writing – review & editing. **Rémi Tyrand:** Formal analysis, Investigation, Methodology, Software, Visualization, Writing – original draft, Writing – review & editing. **Andreas Horn:** Formal analysis, Visualization, Writing – original draft, Writing – review & editing. **Astrid Kibleur:** Software, Writing – review & editing. **Julia Vincentini:** Formal analysis, Writing – review & editing. **André Zacharia:** Resources, Writing – review & editing. **Pierre R. Burkhard:** Data curation, Project administration, Resources, Writing – review & editing. **Shahan Momjian:** Conceptualization, Data curation, Project administration, Resources, Visualization, Writing – review & editing. **Colette Boëx:** Conceptualization, Data curation, Formal analysis, Investigation, Methodology, Project administration, Project administration, Resources, Visualization, Writing – original draft, Writing – review & editing.

Declaration of Competing Interest

The authors declare that they have no known competing financial interests or personal relationships that could have appeared to influence the work reported in this paper.

Appendix A. Supplementary data

Supplementary data to this article can be found online at <https://doi.org/10.1016/j.nicl.2022.102971>.

References

- Abosch, A., Hutchison, W.D., Saint-Cyr, J.A., Dostrovsky, J.O., Lozano, A.M., 2002. Movement-related neurons of the subthalamic nucleus in patients with Parkinson disease. *J. Neurosurg.* 97, 1167–1172.
- Alavi, M., Dostrovsky, J.O., Hodaie, M., Lozano, A.M., Hutchison, W.D., 2013. Spatial extent of β oscillatory activity in and between the subthalamic nucleus and substantia nigra pars reticulata of Parkinson's disease patients. *Exp. Neurol.* 245, 60–71.
- Alexander, G.E., Crutcher, M.D., DeLong, M.R., 1990. Basal ganglia-thalamocortical circuits: parallel substrates for motor, oculomotor, "prefrontal" and "limbic" functions. *Prog. Brain Res.* 85, 119–146.
- Ashburner, J., Friston, K.J., 2005. Unified segmentation. *Neuroimage* 26 (3), 839–851.
- Avants, B., Epstein, C., Grossman, M., Gee, J., 2008. Symmetric diffeomorphic image registration with cross-correlation: evaluating automated labeling of elderly and neurodegenerative brain. *Med. Image Anal.* 12 (1), 26–41.
- Avants, B.B., Tustison, N.J., Song, G., Cook, P.A., Klein, A., Gee, J.C., 2011. A reproducible evaluation of ANTs similarity metric performance in brain image registration. *Neuroimage* 54 (3), 2033–2044.
- Benazzouz, A., Breit, S., Koudsie, A., Pollak, P., Krack, P., Benabid, A.-L., 2002. Intraoperative microrecordings of the subthalamic nucleus in Parkinson's disease. *Mov. Disord.* 17 (S3), S145–S149.
- Boëx, C., Tyrand, R., Horvath, J., Fleury, V., Sadri, S., Corniola, M., Burkhard, P.R., Momjian, S., 2018. What is the best electrophysiologic marker of the outcome of subthalamic nucleus stimulation in Parkinson disease? *World Neurosurg.* 120, e1217–e1224.
- Bot, M., Verhagen, O., Caan, M., Potters, W.V., Dilai, Y., Odekerken, V.J.J., Dijk, J.M., de Bie, R.M.A., Schuurman, P.R., van den Munckhof, P., 2019. Defining the dorsal STN border using 7.0-T MRI: a comparison to microelectrode recordings and lower field strength MRI. *Stereotact. Funct. Neurosurg.* 97 (3), 153–159.
- Brown, P., Oliviero, A., Mazzone, P., Insola, A., Tonali, P., Di Lazzaro, V., 2001. Dopamine dependency of oscillations between subthalamic nucleus and pallidum in Parkinson's disease. *J. Neurosci.* 21 (3), 1033–1038.
- Deffains, M., Holland, P., Moshel, S., de Noriega, F.R., Bergman, H., Israel, Z., 2014. Higher neuronal discharge rate in the motor area of the subthalamic nucleus of Parkinsonian patients. *J. Neurophysiol.* 112 (6), 1409–1420.
- Ewert, S., Pletting, P., Li, N., Chakravarty, M.M., Collins, D.L., Herrington, T.M., Kühn, A.A., Horn, A., 2018. Toward defining deep brain stimulation targets in MNI space: a subcortical atlas based on multimodal MRI, histology and structural connectivity. *Neuroimage* 170, 271–282.
- Fonov, V., Evans, A.C., Botteron, K., Almli, C.R., McKinstry, R.C., Collins, D.L., Brain Development Cooperative, G., 2011. Unbiased average age-appropriate atlases for pediatric studies. *Neuroimage* 54, 313–327.
- Friston, K.J., Holmes, A.P., Worsley, K.J., Poline, J.-P., Frith, C.D., Frackowiak, R.S.J., 1994. Statistical parametric maps in functional imaging: a general linear approach. *Hum. Brain Mapp.* 2 (4), 189–210.
- Gross, R.E., Krack, P., Rodriguez-Oroz, M.C., Reza, A.R., Benabid, A.-L., 2006. Electrophysiological mapping for the implantation of deep brain stimulators for Parkinson's disease and tremor. *Mov. Disord.* 21 (S14), S259–S283.
- Horn, A., Kühn, A.A., 2015a. Lead-DBS: a toolbox for deep brain stimulation electrode localizations and visualizations. *Neuroimage* 107, 127–135.
- Horn, A., Kühn, A.A., 2015b. Lead-DBS: a toolbox for deep brain stimulation electrode localizations and visualizations. *Neuroimage* 107, 127–135.
- Horn, A., Li, N., Dembek, T.A., Kappel, A., Boulay, C., Ewert, S., Tietze, A., Husch, A., Perera, T., Neumann, W.-J., Reiser, M., Si, H., Oostenveld, R., Rorden, C., Yeh, F.-C., Fang, Q., Herrington, T.M., Vorwerk, J., Kühn, A.A., 2019. Lead-DBS v2: towards a comprehensive pipeline for deep brain stimulation imaging. *NeuroImage* 184, 293–316.
- Husch, A., V. Petersen, M., Gemmar, P., Goncalves, J., Hertel, F., 2018. PaCER - A fully automated method for electrode trajectory and contact reconstruction in deep brain stimulation. *Neuroimage Clin.* 17, 80–89.
- Irmen, F., Horn, A., Meder, D., Neumann, W., Pletting, P., Schneider, G., Siebner, H.R., Kühn, A.A., 2019. Sensorimotor subthalamic stimulation restores risk-reward trade-off in Parkinson's disease. *Mov. Disord.* 34 (3), 366–376.
- Isaacs, B.R., Heijmans, M., Kuijff, M.L., Kubben, P.L., Ackermans, L., Temel, Y., Keuken, M.C., Forstmann, B.U., 2021. Variability in subthalamic nucleus targeting for deep brain stimulation with 3 and 7 Tesla magnetic resonance imaging. *Neuroimage Clin.* 32, 102829. <https://doi.org/10.1016/j.nicl.2021.102829>.
- Kim, J., Duchin, Y., Shamir, R.R., Patriat, R., Vitek, J., Harel, N., Sapiro, G., 2019. Automatic localization of the subthalamic nucleus on patient-specific clinical MRI by incorporating 7 T MRI and machine learning: application in deep brain stimulation. *Hum. Brain Mapp.* 40 (2), 679–698.
- Levy, R., Ashby, P., Hutchison, W.D., Lang, A.E., Lozano, A.M., Dostrovsky, J.O., 2002. Dependence of subthalamic nucleus oscillations on movement and dopamine in Parkinson's disease. *Brain* 125, 1196–1209.
- Mallet, L., Polosan, M., Jaafari, N., Baup, N., Welter, M.-L., Fontaine, D., Montcel, S.T., Yelnik, J., Chéreau, I., Arbus, C., Raoul, S., Auouizerate, B., Damier, P., Chabardès, S., Czernecki, V., Ardouin, C., Krebs, M.-O., Bardinet, E., Chaynes, P., Burbaud, P., Cornu, P., Derost, P., Bougerol, T., Bataille, B., Mattei, V., Dormont, D., Devaux, B., Vérin, M., Houeto, J.-L., Pollak, P., Benabid, A.-L., Agid, Y., Krack, P., Millet, B., Pelissolo, A., 2008. Subthalamic nucleus stimulation in severe obsessive-compulsive disorder. *N. Engl. J. Med.* 359 (20), 2121–2134.
- Matsumoto, M., Hikosaka, O., 2009a. Two types of dopamine neuron distinctly convey positive and negative motivational signals. *Nature* 459 (7248), 837–841.
- Matsumoto, M., Hikosaka, O., 2009b. Two types of dopamine neuron distinctly convey positive and negative motivational signals. *Nature* 459 (7248), 837–841.
- Nowacki, A., Nguyen, T.-A.-K., Tinkhauser, G., Petermann, K., Debove, I., Wiest, R., Pollo, C., 2018. Accuracy of different three-dimensional subcortical human brain atlases for DBS-lead localisation. *Neuroimage Clin.* 20, 868–874.
- Parent, A., Hazrati, L.N., 1995. Functional anatomy of the basal ganglia. II. The place of subthalamic nucleus and external pallidum in basal ganglia circuitry. *Brain Res. Rev.* 20, 128–154.
- Pozzi, N.G., Arnulfo, G., Canessa, A., Steigerwald, F., Nickl, R., Homola, G.A., Fato, M.M., Matthies, C., Pacchetti, C., Volkmann, J., Isaías, I.U., 2016. Distinctive neuronal firing patterns in subterritories of the subthalamic nucleus. *Clin. Neurophysiol.* 127 (11), 3387–3393.
- Quiroga, R.Q., Nadasdy, Z., Ben-Shaul, Y., 2004. Unsupervised spike detection and sorting with wavelets and superparamagnetic clustering. *Neural Comput.* 16 (8), 1661–1687.
- Ramayya, A.G., Zaghoul, K.A., Weidemann, C.T., Baltuch, G.H., Kahana, M.J., 2014. Electrophysiological evidence for functionally distinct neuronal populations in the human substantia nigra. *Front. Hum. Neurosci.* 8, 655.
- Rappel, P., Grosberg, S., Arkadir, D., Linetsky, E., Abu Snineh, M., Bick, A.S., Tamir, I., Valsky, D., Marmor, O., Abo Foul, Y., Peled, O., Gilad, M., Daudi, C., Ben-Naim, S., Bergman, H., Israel, Z., Eitan, R., 2020. Theta-alpha oscillations characterize emotional subregion in the human ventral subthalamic nucleus. *Mov. Disord.* 35 (2), 337–343.
- Redgrave, P., Rodriguez, M., Smith, Y., Rodriguez-Oroz, M.C., Lehericy, S., Bergman, H., Agid, Y., DeLong, M.R., Obeso, J.A., 2010. Goal-directed and habitual control in the basal ganglia: implications for Parkinson's disease. *Nat. Rev. Neurosci.* 11 (11), 760–772.
- Richardson, R.M., 2019. Explaining variability in cognitive outcomes from subthalamic stimulation: motor territory stimulation produces nonmotor benefit. *Neurosurgery* 85 (2), E182–E183.
- Rodriguez-Oroz, M.C., Rodriguez, M., Guridi, J., Mewes, K., Chockman, V., Vitek, J., DeLong, M.R., Obeso, J.A., 2001. The subthalamic nucleus in Parkinson's disease: somatotopic organization and physiological characteristics. *Brain* 124, 1777–1790.
- Schönecker, T., Kupsch, A., Kühn, A.A., Schneider, G.-H., Hoffmann, K.-T., 2009. Automated optimization of subcortical cerebral MR imaging-atlas coregistration for improved postoperative electrode localization in deep brain stimulation. *AJNR Am. J. Neuroradiol.* 30 (10), 1914–1921.
- Seifried, C., Weise, L., Hartmann, R., Gasser, T., Baudrexel, S., Szelényi, A., van de Loo, S., Steinmetz, H., Seifert, V., Roeper, J., Hilker, R., 2012. Intraoperative microelectrode recording for the delineation of subthalamic nucleus topography in Parkinson's disease. *Brain Stimul* 5 (3), 378–387.
- Sharott, A., Gulberti, A., Zittel, S., Tudor Jones, A.A., Fickel, U., Munchau, A., Koppen, J.A., Gerloff, C., Westphal, M., Buhmann, C., Hamel, W., Engel, A.K., Moll, C.K.E., 2014. Activity parameters of subthalamic nucleus neurons selectively predict motor symptom severity in Parkinson's disease. *J. Neurosci.* 34 (18), 6273–6285.

- Steigerwald, F., Pötter, M., Herzog, J., Pinsker, M., Kopper, F., Mehdorn, H., Deuschl, G., Volkmann, J., 2008. Neuronal activity of the human subthalamic nucleus in the parkinsonian and nonparkinsonian state. *J. Neurophysiol.* 100 (5), 2515–2524.
- Theodosopoulos, P.V., Marks, W.J., Christine, C., Starr, P.A., 2003. Locations of movement-related cells in the human subthalamic nucleus in Parkinson's disease. *Mov. Disord.* 18 (7), 791–798.
- Vitek, J.L., Zhang, J., Hashimoto, T., Russo, G.S., Baker, K.B., 2012. External pallidal stimulation improves parkinsonian motor signs and modulates neuronal activity throughout the basal ganglia thalamic network. *Exp. Neurol.* 233 (1), 581–586.
- Zaidel, A., Spivak, A., Grieb, B., Bergman, H., Israel, Z., 2010. Subthalamic span of beta oscillations predicts deep brain stimulation efficacy for patients with Parkinson's disease. *Brain* 133, 2007–2021.
- Zaidel, A., Spivak, A., Shpigelman, L., Bergman, H., Israel, Z., 2009. Delimiting subterritories of the human subthalamic nucleus by means of microelectrode recordings and a Hidden Markov Model. *Mov. Disord.* 24 (12), 1785–1793.